ChemComm

Accepted Manuscript

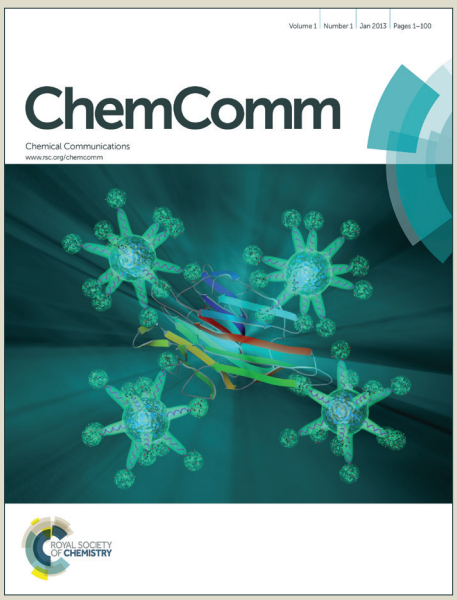

ROYAL SOCIETY OF CHEMISTRY

www.rsc.org/chemcomm

ChemComm

RSCPublishing

COMMUNICATION

2D conglomerate crystallization of heptahelicene

Cite this: DOI: 10.1039/x0xx00000x

Johannes Seibel,[a] Laura Zoppi[b] and Karl-Heinz Ernst*[a,b]

Received 00th January 2012,
Accepted 00th January 2012

DOI: 10.1039/x0xx00000x

www.rsc.org/

Two-dimensional (2D) nucleation and crystallization of the helical aromatic hydrocarbon heptahelicene on the single crystalline copper(100) surface has been studied with scanning tunnelling microscopy. In contrast to previously observed racemic 2D crystals on Cu(111), separation into homochiral domains is observed for Cu(100).

Intermolecular chiral recognition is of paramount importance in materials science and it rules, for example, the outcome of spontaneous resolution in crystallization of enantiomers or the performance of liquid crystal devices. However, understanding the principles of intermolecular recognition is a difficult task and calls for studying appropriate model systems. A promising approach is the investigation of two-dimensional (2D) crystals, that is, the interaction in chiral monolayers on solid surfaces.[1,2] Surface-mediated studies allow in particular the use of scanning tunneling microscopy (STM), a tool providing submolecular resolution. Moreover, surfaces are largely involved in heterogeneous nucleation. Their structure plays therefore an important role for determining the outcome of crystallization such as polymorphism or spontaneous optical resolution of racemic chiral compounds, for example.[1,2]

Molecular helicity is one manifestation of chirality and has important implications in biology or for spin filters based on organic materials.[3] Beyond synthesis of helical hydrocarbons, studying the molecular recognition among 'helicenes' is of great interest nowadays.[4] In particular ortho-annulated, π-conjugated [n]helicenes have attracted much attention due to their outstanding chiroptical properties. In particular the 2D self-assembly and crystallization of heptahelicene ([7]H, $C_{30}H_{18}$, Fig. 1a) has been studied thoroughly.[5-9] [7]H forms heterochiral 2D crystals on Cu(111).[10] That is, the racemic closed-packed monomolecular [7]H layer is comprised of two non-superimposable mirror domains, which have zigzag rows as building blocks. The zigzag rows, in turn, are built-up by pairs of both enantiomers. This '*M*-*P* assignment'¶ in the zigzag row was supported by molecular mechanics calculations.[10] Along the same line, 2-carboxylate-[7]helicene, forms heterochiral nanowires on a calcite surface.[11,12] So far, only the polar 6,13-dicyano-[7]H derivative was found to undergo lateral separation into a 2D conglomerate of homochiral domains.[13] Interestingly, at the Au(111)/liquid interface 5-amino[6]helicene shows coexistence of a 2D conglomerate with the racemate phase.[14] However, spontaneous 2D resolution for an all-carbon helicene has only been reported recently for a pentahelicene on gold(111), which had in addition two benzo rings on the side.[15]

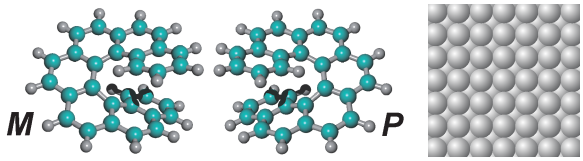

Figure 1. Ball-and-stick models of both [7]H enantiomers and the fcc(100) surface.

Here we demonstrate that non-functionalized [7]H undergoes enantiospecific lateral resolution on the fourfold-symmetric Cu(100) surface (Fig. 1). Four [7]H molecules constitute a homochiral building block, which assembles into homochiral mirror domains at higher coverage. Modeling the STM appearance supports the homochirality of the mirror domains and thus the lateral resolution of the enantiomers. Finally, self-assembly of enantiopure *(M)*-[7]H leads to formation of only one of the two mirror domains observed for the racemate, proving the scenario of optical resolution in the monolayer.

The Cu(100) metal crystal was prepared *in vacuo* by Ar^+ sputtering and annealing to 650 °C. Racemic and *(M)*-[7]H were evaporated from a home made evaporation cell held at 140 °C onto the clean crystal held at room temperature. The absolute handedness was determined via vibrational circular dichroism.[16] After cooling the sample to 50 K, STM (VT Omicron Nanotechnology) images were acquired in constant current mode. The bias voltage refers to the sample; a positive value indicates tunnelling from the tip to the sample. Unit cell models were prepared with HyperChem™ 7.1. The 7[H] molecules were aligned with three C6 rings parallel to the copper surface with the rest of the molecule spiraling away from the surface. Such configuration was found for 7[H] on Cu(111) by photoelectron diffraction.[17] Within the unit cell, the molecules are

rotated by 90° to each other and placed on identical adsorption sites with the proximal ring on top of a copper atom. The final images were rendered using POV-Ray™ Version 3.0. Electronic structure calculations for STM appearance simulation were performed using density functional theory (DFT)[18] in the local density approximation (LDA)[19] with plane wave basis sets and Norm Conserving pseudopotentials,[20] implemented in the Quantum-ESPRESSO package.[21] Calculations are performed at the GAMMA point with an energy cutoff of 100 Ry for the plane-wave basis set. STM images at constant current are calculated within the Tersoff–Hamann approximation.[22]

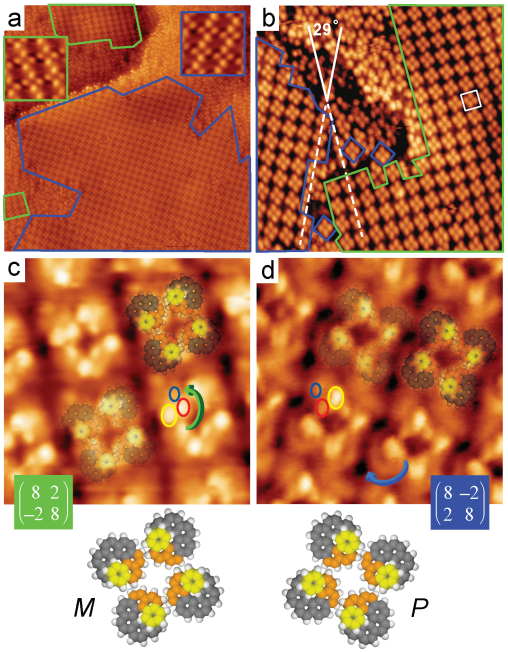

Figure 2. a) STM image (80 nm × 80 nm, U = –2.78 V, I = 42 pA) of a closed-packed layer of *rac*-[7]H on Cu(100). Enantiomorphous (8 –2, 2 8)† and (8 2, –2 8) domains (encircled in blue and green, respectively), consisting of quadruplets of molecules, are observed. At higher magnification [insets, 6 nm × 6 nm, U = –2.61 V, I = 42 pA (green); U = –2.73 V, I = 42 pA (blue)] the quadruplets appear as four-bladed propeller. b) STM image (35 nm × 35 nm, U = –2.73 V, I = 40 pA) near a mirror-domain boundary. The angle between both domains is 29°. A unit cell is indicated as white square. c,d) STM images with submolecular resolution (6 nm × 6 nm, c: U = 0.856 V, I = 179 pA; d: U = –0.773 V, I = 198 pA). Superpositions with semi-transparent models of the quadruplets, with the distal‡ [7]H rings colored in yellow and orange, suggest that the (8 –2, 2 8) domain consists only of *(P)*-[7]H, while the (8 2, –2 8) domain contains only *(M)*-[7]H. The opposite helicity of molecules is indicated by colored arrows, with the tips pointing to the proximal‡ ends.

Self-assembly of *rac*-[7]H on Cu(100) leads to mirror domains in the monolayer (Fig. 2). Instead of zigzag rows or triplets, as observed on Cu(111), here the building block is a molecular quadruplet. The enantiomorphism of the mirror domains is in part based on an oblique tilt angle of one of the adsorbate unit cell vectors with respect to the substrate lattice, *i.e.*, of either –14.5° or +14.5° with respect to the close-packed [011] surface direction. The two enantiomorphous adsorbate lattices have quadratic unit cells with four molecules and are defined as (8 2, –2 8)† and (8 –2, 2 8) in matrix notation.[23] At a first glance, the four molecules of the unit cell appear to be identical, and this is indeed supported by high-resolution STM images (Fig. 2c,d). Depending on the tunneling conditions a single molecule appears as three-lobe pattern with different brightness of the lobes. This allows directly the assignment of the absolute handedness. The (8 2, –2 8) lattice consists only of *(M)*-[7]H and the (8 –2, 2 8) lattice only of *(P)*-[7]H. Matching the molecular model with the images shows that the four molecules in a unit cell are rotated by 90° with respect to each other.

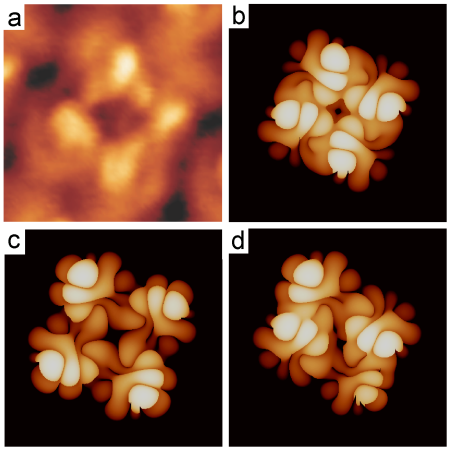

Figure 3. Simulation of the STM appearance. a) Experimental image cut from Fig. 2d. b) Appearance for the *P*-quadruplet. c) Appearance for the *M*-quadruplet. d) Appearance for the *P/M*-quadruplet. See Fig. 4 for the relative arrangements of the molecules.

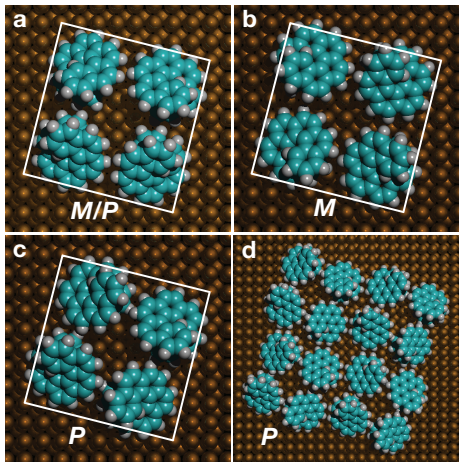

Figure 4. Models for a (8 –2, 2 8) unit cell with two pairs of *M/P*-[7]H- (a), four *(M)*-[7]H- (b) and four *P*-[7]H-molecules (c). Only for *P*-[7]H all molecules occupy the same site in a unit cell and the molecules are related by C_4 symmetry. M/P or M on identical sites do not fit into a (8 –2, 2 8) unit cell (ESI,§ Fig. S1). d) Four unit cells of *P*-[7]H show that this model allows close-packing in an entire domain.

The assignment of a *(P)*-[7]H (8 –2, 2 8) domain is strongly supported by simulations of the STM appearance (Fig. 3) for different close-packing possibilities. Four *P*-enantiomers, four *M*-enantiomers and two pairs of both were placed as quadruplet into a (8 –2, 2 8) cell (Fig. 4). The constant current STM image including LUMO, LUMO+1 and LUMO+2 was calculated for the entire unit cell and compared to experimental STM images obtained when tunneling from the tip into unoccupied states (Fig. 3). The brighter features correspond to the upper part of the molecule and the distal‡ ring appears as intense lobe with a minor intensity located at the

second highest C6 ring. Only the calculated STM image for four *(P)*-[7]H reproduces in good agreement the experimental STM appearance. In particular the position of the brightest lobes and the weaker lobe-intensity between them clearly distinguishes this appearance from the other two possibilities (Fig. 3).

The different close-packing possibilities (Fig. 4) further reveal that four *(P)*-[7]H must constitute the (8 –2, 2 8) cell. If the proximal‡ rings of all four molecules in the unit cell are placed on identical adsorption sites and C_4 symmetry (p4 plane group) is imposed for the pure enantiomers, or C_2 symmetry (p2 plane group) for the racemate, only *(P)*-[7]H fits into a (8 –2, 2 8) cell. Even if different adsorption sites for *M/P*- and *(M)*-[7]H are considered in order to fit four molecules into a (8 –2, 2 8) cell, an extended layer can not be built with these constructions (ESI,§ Fig. S1). Only *(P)*-[7]H quadruplets represent the densest possible packing in the (8 –2, 2 8) domain (Fig. 4d). For the other two possibilities, the molecules would sufficiently overlap with molecules in adjacent cells, imposing a rather strong repulsion (ESI,§ Fig. S1). Even with the high density in the *(P)*-[7]H (8 –2, 2 8) domain such repulsion is avoided, because helicity allows parts of the molecules to slide over/under each other (Fig. 4d).

This result reflects an important aspect of molecular self-assembly at crystalline surfaces: Due to given preferred adsorption sites, molecules establish only dense layers in the limitation of an adsorption grid. This limitation supports stereochemical recognition. Not only intermolecular interaction or the lower dimensionality of the 2D system is important,[24] but in particular the stereochemical interplay of molecule and substrate surface governs the modes of close-packing. Due to the favored adsorption site, the molecules are confronted with a grid that allows only certain intermolecular distances. One step closer imposes substantial repulsion, one step further away a much lower attraction or a much lower density of the 2D crystal. Consequently, this surface recognition mechanism influences the outcome of crystallization. The interatomic distances of the Cu atoms are identical for the (111) surface and the (100) surface. Hence, the differences in symmetry and certain available adsorption sites define a different adsorption-sites-grid, which determines whether a 2D racemate or conglomerate will be formed. For the same reason, pure enantiomers usually 2D-crystallize into only one enantiomorph (single mirror domain) at surfaces.

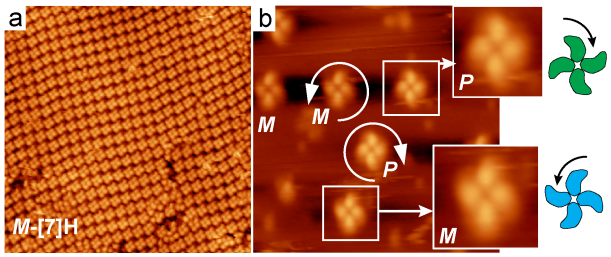

Figure 5. a) STM image (50 nm × 50 nm, U = –1.185 V, I = 29 pA) of *(M)*-[7]H on Cu(100). As ordered structure exclusively the (8 2, –2 8) domain is observed. b) STM image (20 nm × 20 nm, U = –3.079 V, I = 10 pA) showing homochiral quadruplets, as judged by the identically sign of the twist of the tips of the four molecules.

The ultimate proof for the scenario of 2D conglomerate formation on Cu(100) comes from self-assembly of enantiopure *(M)*-[7]H. Exclusively the (8 2, –2 8) domain is observed (Fig. 5a and ESI,§ Fig. S2). Interestingly, the quadruplet motif is already observed at low coverage (Fig. 5b). As for the close-packed layer (insets of Fig. 2a), the clusters appear as four-blade propeller, reflecting again the homochiral composition. This shows that closed-packing is not limited to densely packed monolayers, but also to attractive interactions. However, the mechanism of substrate mediation is the same: attractive interactions are maximized in the limit of a surface grid of favoured adsites. In addition**,** the surface symmetry aligns the molecules in a special manner on the grid. In the case of the fourfold-symmetric Cu(100) surface this mechanism favours conglomerate crystallization of racemic [7]H, in the case of the Cu(111) a racemate crystal.

In conclusion, the self-assembly of *rac*-[7]H and enantiopure *(M)*-[7]H has been studied on Cu(100). The molecules crystallize into homochiral domains and form a 2D conglomerate, while under identical conditions racemate crystallization and heterochiral domains are favoured on the threefold symmetric Cu(111) surface.

Financial support of the Swiss National Science Foundation (SNSF) is gratefully acknowledged.

Notes and references

[a] Empa, Swiss Federal Laboratories for Materials Science and Technology, Überlandstrasse 129, CH-8600 Dübendorf, Switzerland. Tel.: +41 58 765 43 63
E-mail: karl-heinz.ernst@empa.ch
[b] Department of Chemistry, University of Zurich, CH-8057 Zürich, Switzerland

¶ According to the Cahn-Ingold-Prelog convention, the denominators for left- and right-handed helical molecules are M and P (minus and plus).

† The (2×2) transformation matrix, linking the adsorbate lattice vectors (b_1, b_2) to the substrate lattice vectors (a_1, a_2) *via* $b_1 = m^{11}a_1 + m^{12}a_2$ and $b_2 = m^{21}a_1 + m^{22}a_2$, is written here in the form (m^{11} m^{12}, m^{21} m^{22}).

‡ We use *proximal* and *distal* here for the parts of a molecule farthest away from – and closest to – the surface, respectively.

§ Electronic Supplementary Information (ESI) available: Molecular packing models and STM image. See DOI: 10.1039/c000000x/

1. K.-H. Ernst, *Phys. Status Solidi B*, 2012, **249**, 2057–2088.
2. R. Raval, *Chem. Soc. Rev.*, 2009, **38**, 707–721.
3. R. Naaman and D. H. Waldeck, *J. Phys. Chem. Lett.*, 2012, **3**, 2178–2187.
4. Y. Shen and C.-F. Chen, *Chem. Rev.*, 2012, **112**, 1463–1535.
5. R. Fasel, M. Parschau, and K.-H. Ernst, *Angew. Chem. Int. Ed.*, 2003, **42**, 5178–5181.
6. M. Parschau, R. Fasel, and K.-H. Ernst, *Crystal Growth & Design*, 2008, **8**, 1890–1896.
7. K.-H. Ernst, M. Neuber, M. Grunze, and U. Ellerbeck, *J. Am. Chem. Soc.*, 2001, **123**, 493–495.
8. M. Parschau, U. Ellerbeck, and K.-H. Ernst, *Colloids and Surfaces A: Physicochemical and Engineering Aspects*, 2010, **354**, 240–245.
9. K. H. Ernst, Y. Kuster, R. Fasel, C. F. McFadden, and U. Ellerbeck, *Surf. Science*, 2003, **530**, 195–202.
10. R. Fasel, M. Parschau, and K.-H. Ernst, *Nature*, 2006, **439**, 449–452.
11. P. Rahe, et. al, *J. Phys. Chem. C*, 2010, **114**, 1547–1552.
12. C. M. Hauke, et. al., *J. Phys. Chem. C*, 2012, **116**, 4637–4641.
13. M. Stöhr, et. al., *Angew. Chem. Int. Ed.*, 2011, **50**, 9982–9986.
14. T. Balandina, M. W van der Meijden, O. Ivasenko, D. Cornil, J. Cornil, R. Lazzaroni, R. M. Kellogg, and S. De Feyter, *Chem. Commun. (Camb.)*, 2013, **49**, 2207–2209.
15. J. Seibel, O. Allemann, J. S. Siegel, and K.-H. Ernst, *J. Am. Chem. Soc.*, 2013, **135**, 7434–7437.
16. T. Bürgi, A. Urakawa, B. Behzadi, K.-H. Ernst, and A. Baiker, *New J. Chem.*, 2004, **28**, 332–334.
17. R. Fasel, A. Cossy, K. H. Ernst, F. Baumberger, T. Greber, and J. Osterwalder, *J. Chem. Phys.*, 2001, **115**, 1020–1027.
18. P. Hohenberg and W. Kohn, *B864*, 1964.
19. W. Kohn and L. J. Sham, *Phys. Rev.*, 1965, **140**, A1133–A1138.
20. D. R. Hamann, M. Schlüter, and C. Chiang, *Phys. Rev. Lett.*, 1979, **43**, 1494–1497.
21. P. Giannozzi, et. al. *J Phys Condens Mat.*, 2009, **21**, 395502.
22. J. Tersoff and D. R. Hamann, *Phys. Rev. B*, 1985, **31**, 805–813.
23. L. Merz and K.-H. Ernst, *Surf. Science*, 2010, **604**, 1049–1054.
24. I. Kuzmenko, I. Weissbuch, E. Gurovich, L. Leiserowitz, and M. Lahav, *Chirality*, 1998, **10**, 415–424.